# Shipborne Dual-Doppler Operations during TOGA COARE: Integrated Observations of Storm Kinematics and Electrification

Walter A. Petersen,* Robert C. Cifelli,+,# Steven A. Rutledge,*
Brad S. Ferrier,+,@ and Bradley F. Smull&

## ABSTRACT

Shipborne Doppler radar operations were conducted over the western Pacific warm pool during TOGA COARE using the Massachusetts Institute of Technology and NOAA TOGA C-band Doppler radars. Occasionally the ships carrying these radars were brought to within 50 km of each other to conduct coordinated dual-Doppler scanning. The dual-Doppler operations were considered a test of the logistical and engineering constraints associated with establishing a seagoing dual-Doppler configuration. A very successful dual-Doppler data collection period took place on 9 February 1993 when an oceanic squall line developed, intensified, and propagated through the shipborne dual-Doppler lobes. Later on the same day, NOAA P-3 aircraft sampled a more intense squall line located approximately 400 km to the southeast of the shipborne operations. This study provides an overview of the shipborne dual-Doppler operations, followed by a comparison of the kinematic and precipitation structures of the convective systems sampled by the ships and aircraft. Special emphasis is placed on interpretation of the results relative to the electrical characteristics of each system.

Soundings taken in the vicinity of the ship and aircraft cases exhibited similar thermodynamic instability and shear. Yet Doppler radar analyses suggest that the aircraft case exhibited a larger degree of low-level forcing, stronger updrafts, more precipitation mass in the mixed-phase region of the clouds, and a relatively higher degree of electrification as evidenced by lightning observations. Conversely, convection in the ship case, while producing maximum cloud-top heights of 16 km, was associated with relatively weaker low-level forcing, weaker vertical development above the –5°C level, moderate electric fields at the surface, and little detectable lightning. Differences in the kinematic and precipitation structures were further manifested in composite vertical profiles of mean convective precipitation and vertical motion. When considered relative to the electrical properties of the two systems, the results provide further circumstantial evidence to support previously hypothesized vertical velocity and radar reflectivity thresholds that must be exceeded in the 0° to –20°C regions of tropical cumulonimbi prior to the occurrence of lightning.

*Department of Atmospheric Science, Colorado State University, Fort Collins, Colorado.
+Joint Center for Earth Systems Technology, University of Maryland—Baltimore County, Baltimore, Maryland.
#Laboratory for the Atmospheres, NASA/Goddard Space Flight Center, Greenbelt, Maryland.
@Mesoscale Atmospheric Processes Branch, Laboratory for the Atmospheres, NASA/Goddard Space Flight Center, Greenbelt, Maryland.
&NOAA/National Severe Storms Laboratory/Joint Institute for Study of the Atmosphere and Ocean, University of Washington Seattle, Washington.
*Corresponding author address:* Dr. Walter A. Petersen, Department of Atmospheric Science, Colorado State University, Fort Collins, CO 80523.
In final form 15 July 1998.


## 1. Introduction

From November 1992 to March 1993, the Tropical Ocean Global Atmosphere Coupled Ocean–Atmosphere Response Experiment (TOGA COARE; Webster and Lukas 1992) was conducted in the warm-pool region of the western Pacific Ocean. The scientific goals of TOGA COARE focused on the study of interactions between the warm ocean surface and the tropical atmosphere over a variety of scales. Because atmospheric convection plays such a key role in the transfer of heat, momentum, and water substance (vapor and liquid) between the troposphere and the ocean, the scientific objectives of TOGA COARE required 1) accurate measurements of rainfall (Short et al.

1997); and 2) documentation of the life cycle, organization, and three-dimensional kinematic and precipitation structures associated with cumulonimbus convection occurring in the warm-pool region.

Earlier field programs such as the Global Atmospheric Research Program (GARP) Atlantic Tropical Experiment provided many new insights into the precipitation structure and life cycle of tropical convection using radar reflectivity data collected by incoherent shipborne radars (e.g., Houze and Cheng 1977; Leary and Houze 1979; Szoke et al. 1986; Szoke and Zipser 1986). More recently, airborne Doppler radars have been used to study *both* precipitation structures and 3D wind fields over remote regions of the Tropics (e.g., Marks and Houze 1984; Jorgensen et al. 1991, 1996, 1997). Indeed, Doppler radars operated from airborne platforms such as the National Oceanic and Atmospheric Administration (NOAA) WP-3D, National Center for Atmospheric Research (NCAR) Electra, and National Aeronautics and Space Administration DC-8 aircraft were key components in the sampling of a variety of convective systems over the warm pool during COARE (e.g., Yuter et al. 1995; Hildebrand et al. 1996; Jorgensen et al. 1997). One limitation of airborne platforms, however, is the amount of time that can be spent on station actually sampling convection (typically 4–8 h). Additionally, during TOGA COARE, logistics and imperfect forecasts precluded the aircraft from sampling the early development of many (but not all) convective systems. Hence, the complementary missions of *continuously* mapping rainfall over the warm-pool region, while coincidentally observing the *complete* life cycle of long-lived mesoscale convective systems (MCSs), both important to achieving the scientific goals of TOGA COARE, were not attainable using *only* airborne platforms.

To facilitate the collection of a continuous record of rainfall (e.g., Short et al. 1997), and to document the life cycle, organization, precipitation, and kinematic structures of tropical convection over the western Pacific warm pool (e.g., Rickenbach and Rutledge 1998; DeMott and Rutledge 1998a,b), two C-band Doppler radars (characteristics described in Short et al. 1997) were deployed on board the research vessels *John V. Vickers* [Massachusetts Institute of Technology (MIT) radar] and the *Xiang Yang Hong 5* (*PRC5*; NOAA TOGA radar). Each of these radars were on station in the COARE intensive flux array (IFA) for three 30-day periods, located at the nominal positions of 2°S, 156°15′E and 2°5′S, 155°5′E,[1] respectively (Fig. 1). While deployed, both radars collected data 24 h day$^{-1}$ with the exception of down time for maintenance and calibration.

During February 1993, the ships were repositioned several times to form an approximate 50-km baseline for the purpose of conducting dual-Doppler operations with the ultimate goal of sampling the three-dimensional kinematic structure of an oceanic MCS. At the most basic level, the coordinated radar sampling was undertaken as an experiment to examine the feasibility of conducting successful dual-Doppler operations at sea. Herein we present a brief description of these first coordinated dual-Doppler operations, followed by an overview of one particular case; a deep squall line that developed in the dual-Doppler lobes of the shipboard radars on 9 February 1993. We then compare the shipborne dual-Doppler squall line observations (hereafter referred to as the "ship" case) to airborne Doppler radar observations (NOAA P-3) of a more intense linear MCS (hereafter referred to as the "aircraft" case) that occurred slightly southeast of the IFA on the same day (e.g., Smull et al. 1994; Smull et al. 1996; Lee and Hildebrand 1995). Special emphasis will be placed on the interpretation of kinematic and precipitation structures associated with the two MCSs relative to their respective electrical characteristics as observed by the COARE Advanced Lightning Direction Finder network (ALDF; Petersen et al. 1996; Orville et al. 1997) and an electric field mill operated on board the R/V *Vickers* (Petersen et al. 1996).

*Radar stabilization*

Since the MIT and TOGA Doppler radars were situated on ships, it was necessary to account for the instantaneous heading, roll, and pitch, as well as time derivatives of these quantities (Rutledge et al. 1993). This was accomplished by stabilizing the radar antenna through the use of an inertial navigation unit (INU) mounted on each of the radar antenna pedestals. The INU sensed roll, pitch, and heading of the antenna associated with the degrees of freedom of the ship's motion. A Global Positioning System (GPS) receiver provided latitude, longitude, and time information. The INU and GPS information were fed to a "grid computer" and subsequently passed to the radar con-

[1]The nominal position of the *PRC5* varied slightly as a function of the observation period.

trol interface (RCI). The RCI controlled the antenna such that the antenna appeared to be fixed to a horizontal plane on the earth's surface. The stabilization technique relied upon rapid updates of the antenna position to maintain desired azimuth and elevation angles; hence, the INU information was passed to the RCI at a data rate of 200 Hz. Real-time estimates of radial velocity were corrected for ship motion prior to being passed to the recording media or used in product generation. Tests of the stabilization hardware and software were conducted on components to the TOGA radar, which was installed on a ship simulator at Martin Marietta Corporation in Baltimore, Maryland, prior to field deployment. The antenna was directed to a fixed point in space and required to maintain that point when the simulator was rocked back and forth (rolls of approximately 10° were simulated). Further tests of the stabilization were conducted at sea during COARE by pointing the antenna at the sun during various sea states. Based on the above tests, the antenna pointing accuracy was estimated to be 0.1°.

Position errors in the ship radar data occurred due to a Schuler oscillation in the INU with a period of 84.4 min (Leary et al. 1993). This low-frequency oscillation is present in the $u$ and $v$ components of the ship's velocity data. The amplitude of the oscillation ranged from 0.25 to 2 m $s^{-1}$ for the MIT radar and from 1 to 7 m $s^{-1}$ for the TOGA radar. The magnitude was larger for the TOGA radar, since the INU on that platform was manually updated with the GPS position at time intervals of 1–2 h due to a failure in the grid computer. However, during dual-Doppler operations the TOGA radar INU was updated at 15-min intervals (Short et al. 1997), thereby reducing the amplitude of the Schuler oscillation. For the MIT radar, the INU position updating procedure was completed automatically at approximately 1-min intervals throughout TOGA COARE.

## 2. Overview of the ship-based dual-Doppler operations

The MIT and TOGA radars were operated in a dual-Doppler scanning mode on three separate occasions during February 1993 (6–7 February, 9 February, and 12–13 February). These periods of synchronized scanning lasted for approximately 10–24 h, depending on the intensity of convective activity observed during the sampling period. Due to the logistics involved in repositioning both ships for dual-Doppler operations (e.g., a time period of nearly 5 h was required to allow for ship engine warm-up, retrieval of deployed scientific instrumentation, and ferry time), and due to rapidly changing atmospheric conditions in the IFA (e.g., transitions from suppressed to convectively active within a time span of 1–2 h), the decision to initiate dual-Doppler operations necessarily depended on a limited ability to forecast meteorological conditions in the IFA at least 12 h in advance. In this sense the dependence on accurate forecasts was comparable to the aircraft operations. Hence "go" or "no-go" decisions regarding dual-Doppler operations were ultimately left to the discretion of radar scientists aboard the R/V *Vickers* and *PRC5* (communications via HF radio, fax, and phone) and were based on operations center daily forecasts and synoptic summaries, available surface meteorological data, radar and sounding data, and visual observations. Of the three occasions that dual-Doppler operations were initiated, the most productive day of coordinated sampling occurred on 9 February 1993. From a purely logistical viewpoint, the coordinated data collections of 6–7 February and 12–13 February could also be considered a success. However, little or no convection occurred in the dual-Doppler coverage area during 10 h of operations on 6–7 February, and hardware failure terminated dual-Doppler operations on 12–13 February.

### *a. Dual-Doppler sampling on 9 February 1993*

On 9 February 1993 atmospheric conditions appeared favorable for the development of convective activity in the IFA (see section 3) and the radar crews decided to conduct dual-Doppler operations. It was decided that the ships would be positioned along a northeast–southwest baseline (Fig. 1) in the vicinity of 1.7°S, 155°E. The positioning and maintenance of the radar baseline were accomplished by allowing the *PRC5* to drift while the R/V *Vickers* continually repositioned to maintain the baseline at a fixed heading and distance from the *PRC5*. The baseline was initially set at 47 km with the MIT (TOGA) radar located on the northeast (southwest) end of the baseline (Fig. 1). The orientation of the baseline was selected in advance in order to maximize the temporal coverage of convective systems, which, earlier in the day, had shown a tendency to move northwest to southeast through the dual-Doppler lobes sampled by the radars and roughly perpendicular to the radar baseline in Fig. 1. However, the MCS sampled on 9 February moved through the dual-Doppler domain with exactly the opposite orientation (i.e., the line was oriented roughly perpendicular

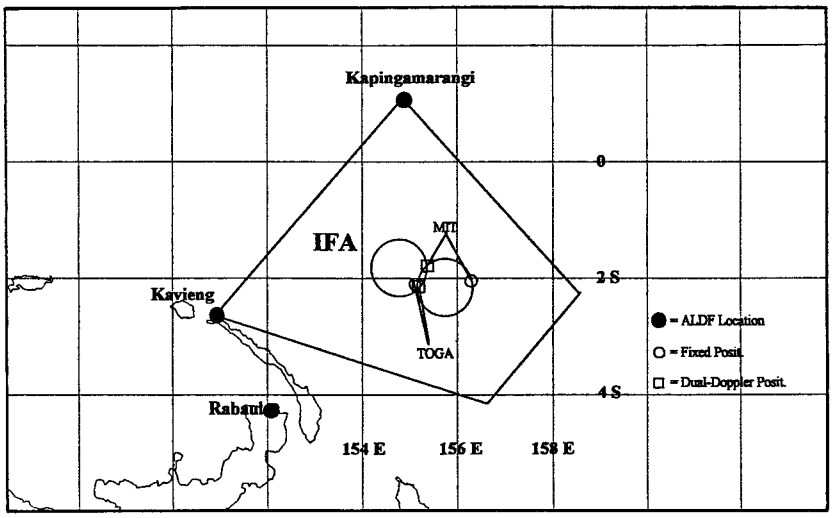


FIG. 1. Map of the TOGA COARE IFA. The relative positions of the MIT and TOGA radars during dual-Doppler operations on 9 February 1993 are indicated by an open square (□). The nominal locations of each radar in February of 1993 are indicated by an open circle (○). Antenna locations in the COARE ALDF network are indicated by a filled circle (●).

to the baseline and moved approximately parallel to the baseline), emphasizing the highly variable nature of convective activity in the IFA.

Synchronized volume scanning at 10-min intervals began around 0430 UTC and continued until approximately 1800 UTC. Because both ships implemented preprogrammed full volume scans (see Short et al. 1997) and because the scan sequence on both radars was controlled by GPS clocks, synchronization of the volume scan times for the MIT and TOGA radars was maintained to within 30 s.

*b. Analysis methodology for the 9 February "ship" case*

A total of 15 volumes of radar data collected at 10-min intervals and covering approximately 2.5 h of storm evolution[2] has been analyzed. Prior to performing a dual-Doppler synthesis, a +2.4 dB gain adjustment was added to the MIT radar reflectivity data as discussed by Ferrier et al. (1995). No corrections were applied to the raw radial velocity data to correct for Schuler oscillations (e.g., Leary 1993; Matejka and Lewis 1997). This is because frequent INU updates (every 10–15 min) were performed during the sampling period, resulting in velocity biases that were within the uncertainty of the radial velocity measurements (~1 m $s^{-1}$).

The radar data were subsequently interpolated to a Cartesian grid (1-km horizontal grid spacing; 0.5-km vertical spacing) using a Cressman weighting scheme with a 1.5-km radius of influence in the horizontal and a 1.0-km radius in the vertical. To recover the three-dimensional wind field, radial-velocity data from the MIT and TOGA radars were used as input to a "two equation" synthesis (Ray et al. 1980) as coded in the CEDRIC [Custom Editing and Display of Reduced Information in Cartesian space; Mohr and Miller (1983)] software package. For each CEDRIC run, a one-step Leise filter and patching function were applied to the horizontal winds after the initial synthesis to smooth the resulting wind field. The vertical velocity was set to zero at a distance of 500 m above the highest measured divergence in each grid column. Vertical air motion was calculated by integrating the anelastic form of the mass continuity equation downward from the top boundary condition in order to take advantage of the density weighting and to minimize errors in the vertical motion field. In the final step of the analysis, a variational adjustment scheme following O'Brien (1970) was used to redistribute mass through the grid column to account for uncertainties in the divergence estimates. However, due to poor sampling of cloud-top and/or low-level divergence by the radars, substantial errors in the vertical draft structure can exist in the dual-Doppler analyses (cf. Jorgensen et al. 1996).

## 3. Storm environment on 9 February 1993

Surface streamline and satellite analyses for 9 February 1993 (Asencio et al. 1993; Bond and Alexander 1994) indicated an elongated region of confluence and associated convection situated within and southeast of the IFA, which extended east toward the date line. The analyses suggest that low-level confluence was stronger southeast of the IFA in the vicinity of the aircraft case (though surface wind ob-

[2]The TOGA radar was inoperative for a 20-min period between 0950 and 1010 UTC.

servations were sparse), which occurred later in the day near 4.5°S, 159°E. Sounding data collected aboard the R/V *Vickers* at 0600 UTC (Fig. 2a) indicated the presence of significant convective available potential energy (CAPE) (2000 J kg$^{-1}$) and very little convective inhibition (CIN) (~4 J kg$^{-1}$) in the prestorm environment. Moderate low-level westerlies and strong upper-level easterlies existed in the environment of the ship case (Fig. 2a). The low-level (1000–800 mb) shear vector was directed from 240° at 9 m s$^{-1}$. The midlevel shear vector [800–400 mb; e.g., Alexander and Young (1992); LeMone et al. (1998)] was oriented from the east-southeast with a direction of 101° and magnitude of 16.5 m s$^{-1}$. A composite "inflow" sounding (Fig. 2b) constructed for the aircraft case (cf. LeMone et al. 1998) yielded a CAPE value similar to that of the ship sounding, but possessed a CIN of 0 J kg$^{-1}$ and generally higher specific humidity above the top of the mixed layer (~950 mb; Fig. 2b). The direction and speed of the low-level (midlevel) shear vector (cf. LeMone et al. 1998) computed for the aircraft sounding was approximately 220° at 6.7 m s$^{-1}$ (81° at 16.5 m s$^{-1}$).

## 4. Shipborne dual-Doppler observations of a tropical oceanic squall line

The MCS sampled by the shipboard radars (Figs. 3–7) on 9 February 1993 organized along a boundary that emanated from the edge of a decaying convective system located ~100 km to the south of the two shipboard radars. In the earliest stages of the convective life cycle, convective cells were initiated northwest to southeast along the boundary as it propagated into the region of dual-Doppler coverage between 0900 and 0930 UTC (Fig. 3). Development of a 150–200-km-long broken (occasionally solid) line of convective cells ensued, with the system assuming an orientation of 140° early in its life cycle (Fig. 3) and transitioning to an orientation of 110° (e.g., Fig. 4a) during its mature stage [orientation conven-

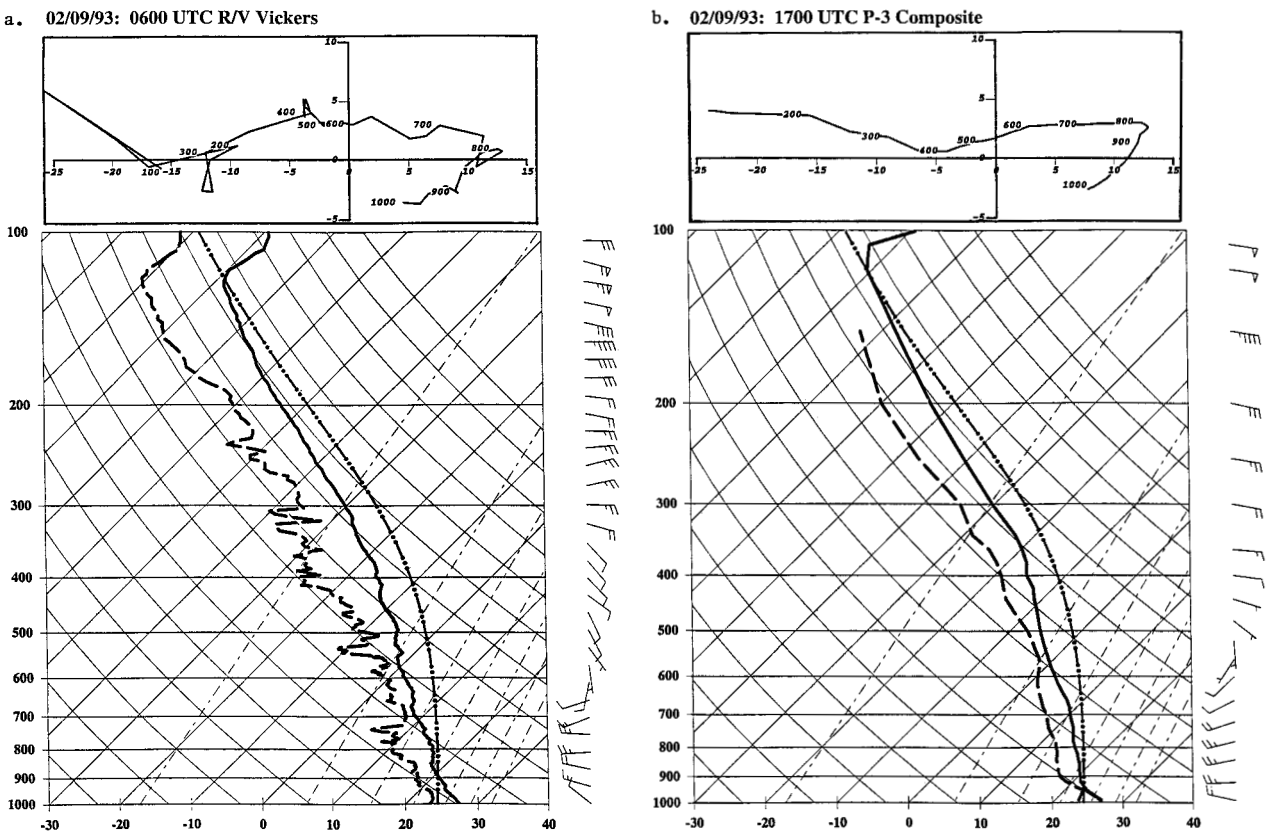


FIG. 2. (a). Skew *T* plot and hodograph (top) for the R/V *Vickers* sounding taken at 0600 UTC 9 February 1993. Bold–solid (dashed) lines indicate the temperature (dewpoint) profile. The dot–dash lines represent a mean mixed layer (50-mb depth) pseudoadiabat (~355 K). Wind barbs (m s$^{-1}$) are indicated on the right side of the diagram, full barbs = 5 m s$^{-1}$, half barbs = 2.5 m s$^{-1}$, and flags = 25 m s$^{-1}$. Hodograph winds (m s$^{-1}$) are plotted as *u* (abscissa) and *v* (ordinate) components with pressure levels (mb) indicated on the trace. (b) As in (a) except aircraft case composite profile.

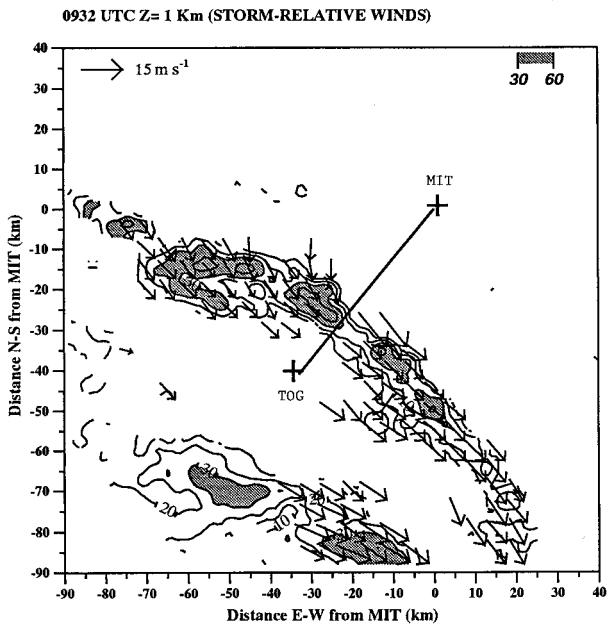


FIG. 3. Constant altitude plan position indicator (CAPPI) of "ship case" radar reflectivities and storm-relative winds (210° at 10 m $s^{-1}$) at an elevation of 1 km for 0932 UTC 9 February 1993. Radar reflectivity is contoured at an interval of 10 dBZ. Reflectivity values greater than 30 dBZ are shaded. The locations of the MIT and TOGA radars, and the approximate dual-Doppler baseline, are also indicated. The vector scale is indicated in upper left-hand corner of the figure.

tion as in Alexander and Young (1992)]. Note that the convective line was oriented nearly *perpendicular* (within 10°) to the low-level shear vector early in its life cycle (240° at 9 m $s^{-1}$) but assumed an orientation nearly *parallel* to the stronger *midlevel* shear vector (101° at 16.5 m $s^{-1}$) during its mature stage. The degree to which the MCS influenced the orientation of the low-level shear vector for several hours after 0600 UTC is not known; however, a sounding taken on the trailing edge of the system at 1200 UTC suggests that momentum transports associated with the MCS eliminated the low-level shear in the lowest 3 km of the troposphere while having little effect on the midlevel shear.

For the majority of the observation period, the squall line propagated toward the north-northeast (from a direction of 210°) at an average speed of 10 m $s^{-1}$. Individual convective cells embedded in the squall line tended to propagate eastward in a discrete fashion along the convective line and roughly parallel to the environmental winds between 900 and 750 mb (Fig. 2a). Near 1042 UTC (Fig. 4a) the convective line and associated gust front reached the location of the MIT radar, producing a 3°C drop in surface temperature and wind gusts of 10–15 m $s^{-1}$. The reflectivities and storm-relative winds shown in Fig. 4a are characteristic of the horizontal morphology associated with the MCS as it began to enter the mature stage. In general, the system was associated with relatively weak low-level confluence of the wind

(a)

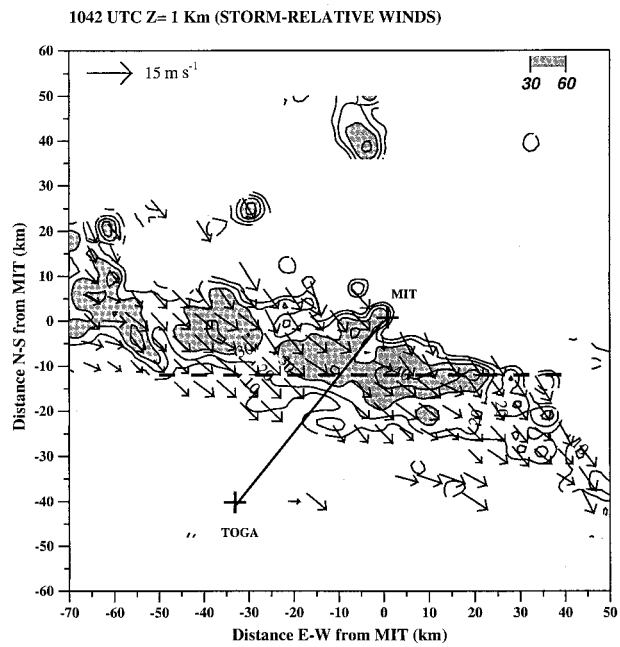


(b)

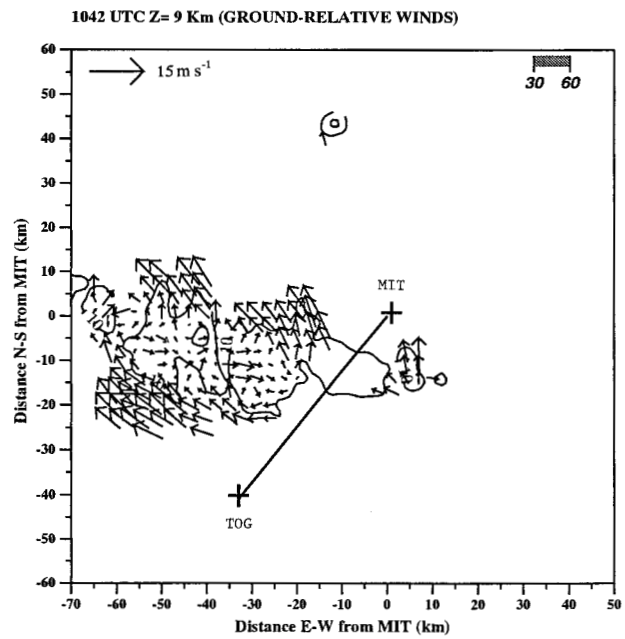


FIG. 4. (a) As in Fig. 3 but for 1042 UTC. Dashed line indicates orientation of cross section in Fig. 7a; (b) as in (a) but for *ground-relative* winds at an elevation of 9 km (see text regarding use of ground- vs storm-relative wind).

on the mesoscale, with regions of marked convergence occasionally being observed in association with individual convective cells.

Above the 7-km level (Fig. 4b) ambient easterly flow (Fig. 2) was diverted around the deeper convective towers, producing a wake that appeared to influence the vertical orientation of updraft cores on the western side of the MCS (note that *ground-relative* winds are presented in Fig. 4b to better elucidate the effect that convection had on the environmental flow and momentum transports). For example, updrafts and convective reflectivity cores in the storm tended to tilt rearward (e.g., toward the southwest) relative to the northeastward movement of the system. However, blocking of the ambient easterly flow aloft by convective updrafts located on the southeastern side of the MCS allowed updraft carrying low-level westerly momentum located on the northwestern side of the storm to occasionally tilt toward the southeast upon reaching the upper levels of the system. This resulted in a vertical motion and precipitation structure that was highly three-dimensional in character. Transport of westerly momentum between the lower and upper levels of the squall line is evident in Fig. 4b along the longitudinal axis of the convective line.

Approximately 1 h later (1132 UTC; Fig. 5a) the MCS consisted of a broken convective line with a trailing region of stratiform precipitation. During this period, the eastern end of the convective line weakened considerably while the western end produced the deepest convection (16-km echo tops; Fig. 5b) observed in the 2.5-h sampling period. The vertical structure of the horizontal flow (Fig. 5b) consisted of strong line-parallel components consistent with the observed movement of individual convective cells. For example, the east–west cross section shown in Fig. 5b indicates the presence of an eastward (down band) propagating gust front and associated northwesterly surge of momentum (e.g., $x = -30$ to $-35$), produced by a particularly intense portion of the convective band located along Y = 20 in Fig. 5a.

As the MCS transitioned from a mature to dissi-

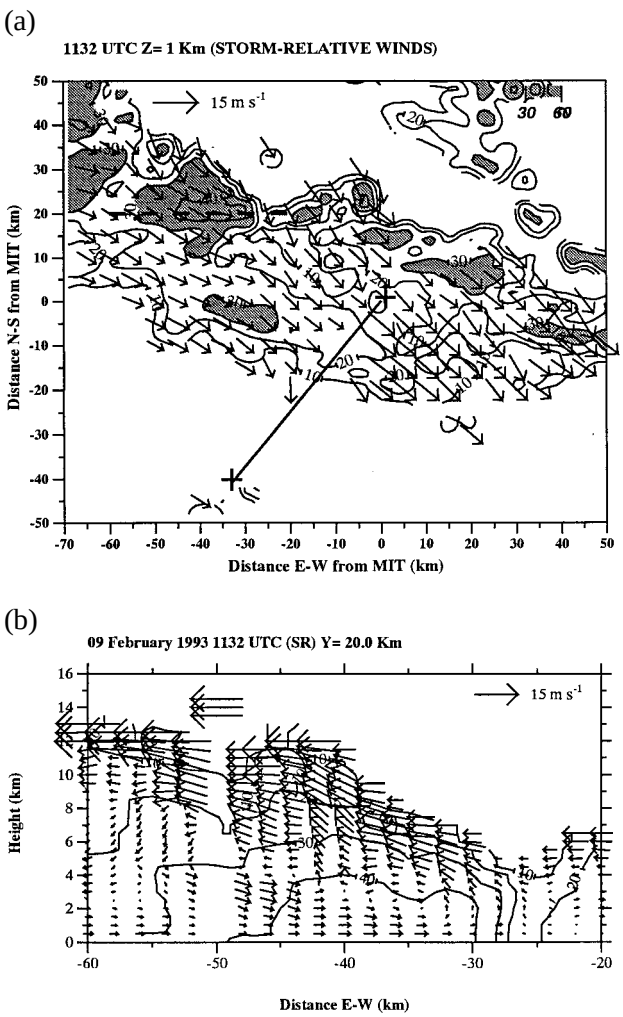


FIG. 5. (a) As in Fig. 3 but for 1132 UTC. Bold–dashed line indicates orientation of cross section in (b). (b) East–west vertical cross section of radar reflectivity (contoured at a 10-dB*Z* interval) and storm-relative winds for (a). Cross section is taken along the E–W-oriented bold–dashed line in (a) at the N–S coordinate $Y = 20$ km. Height is indicated in kilometers on the ordinate; E–W distance from the MIT radar in km is indicated on the abscissa.

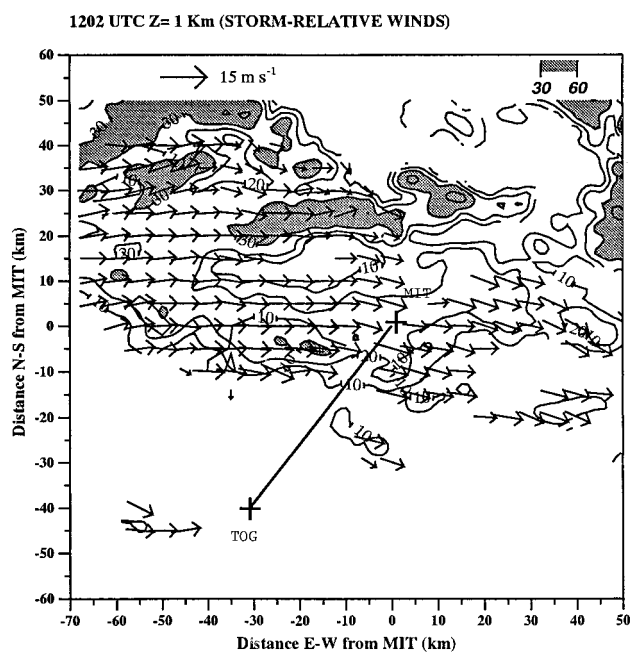


FIG. 6. As in Fig. 3 but for 1202 UTC.

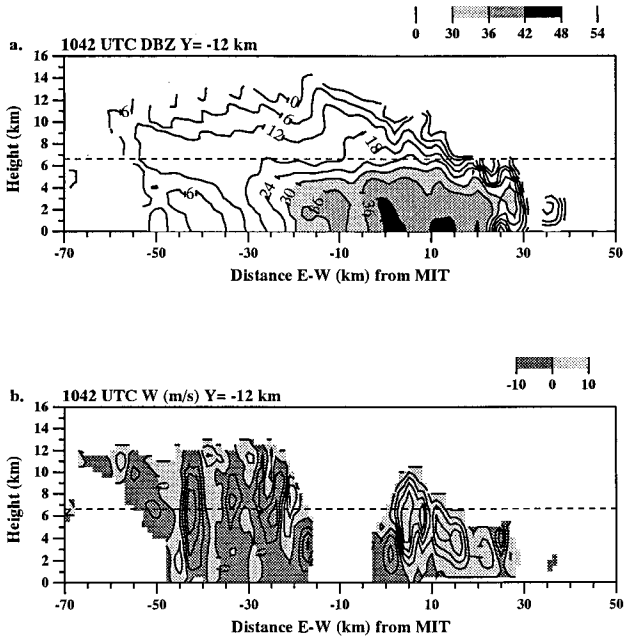


FIG. 7. East–west vertical cross section of (a) radar reflectivity and (b) vertical velocity, taken at $Y = -12$ km, 1042 UTC (see Fig. 3). Values of radar reflectivity (vertical velocity) are contoured at 6-dB$Z$ (1 m s$^{-1}$) intervals and reflectivities greater than 30 dB$Z$ are shaded. Light (dark) shading in (b) indicates upward (downward) motion. The dashed line indicates the approximate elevation of the ambient −10°C isotherm.

pating stage within the dual-Doppler lobes (1200 UTC; Fig. 6), the northeastward progression of the squall line decreased, the western end of the convective line became weak and disorganized, and the system became dominated by stratiform precipitation that expanded on the western side of the MCS in the vicinity of dissipating convection. Interestingly, the previously weakened eastern end of the convective line, which had moved well outside the area of dual-Doppler coverage by 1200 UTC, appeared to reintensify as it moved northeast. The remaining western section of the MCS moved completely out of the dual-Doppler lobes by 1245 UTC. Based on the stage of the MCS life cycle at 1245 UTC, and on the constraints associated with moving both ships to a new location, a decision was made to hold the original baseline position instead of moving the ships to sample the dissipating stage of the MCS.

*Vertical structure and electrification*

To further examine the vertical structure of the MCS, representative alongline vertical cross sections of radar reflectivity and vertical velocity are presented in Figs. 7a,b (1042 UTC). Reflectivities greater than 30 dB$Z$ (Figs. 5b, 7a) were confined to elevations below the 6.5-km level (−10°C) while radar echo tops often exceeded 14–15 km. Vertical velocities were relatively weak in the convective line (Fig. 7b) with updraft maxima of 3–5 m s$^{-1}$ present below the freezing level (~5 km), and 6–9 m s$^{-1}$ present above the 7-km level (e.g., Fig. 5b). Maximum downdrafts were found in the midlevels of the system and were generally ≤ 3 m s$^{-1}$. Consistent with previous observations of tropical oceanic convection (e.g., Orville and Spencer 1979; Zipser 1994; Petersen et al. 1996), little or no lightning was detected in association with the ship case, either visually (it was dark during the entire sampling period) or by the COARE ALDF network. The peak vertical electric field measured at the location of the R/V *Vickers* reached maximum values of 5 kV m$^{-1}$ during passage of the convective line, and only one electric field transient, possibly an intracloud lightning flash, was detected by the field mill during the entire event. Though clouds in the convective line were clearly deep (e.g., Figs. 5b, 7a,b), the presence of reflectivity values less than 30 dB$Z$ in the −10° to −40°C region of the squall line suggests the presence of reduced mixed-phase precipitation ice processes in the cold region of the clouds and, hence, a weaker charge generation process (Takahashi 1978; Saunders et al. 1991; Rutledge et al. 1992; Williams et al. 1992; Randell et al. 1994; Zipser and Lutz 1994; Petersen et al. 1996).

One possible explanation for the absence of a robust mixed-phase ice process and associated lightning activity in this case is suggested by the three-dimensional view of the MCS shown in Fig. 8. More specifically, note in Fig. 8 the separation between moderate updrafts (e.g., ≥ 5 m s$^{-1}$) situated *above* the freezing level, and significant hydrometeor mass (e.g., reflectivities of 30–40 dB$Z$ or greater) situated *below* the freezing level. Analysis of the squall-line vertical structure, as illustrated in Figs. 5b, 7a,b, and 8, suggests that most of the condensation leading to precipitation formation and associated water loading of the updrafts occurred well below the freezing level. As the weakened updrafts ascended to the freezing level, the combined effects of condensate unloading and the release of latent heat as the remaining condensate froze likely provided the buoyancy required for acceleration of the updrafts above the freezing level (e.g., the top of the 40-dB$Z$ isosurface stopped abruptly between the 0° and −5°C levels; Fig. 8). Even in the *most intense* convention sampled during the ship case (Figs. 5b, 9a,b), small areas containing 30–40-dB$Z$ values approached the height of the −10°C level only sporadi-

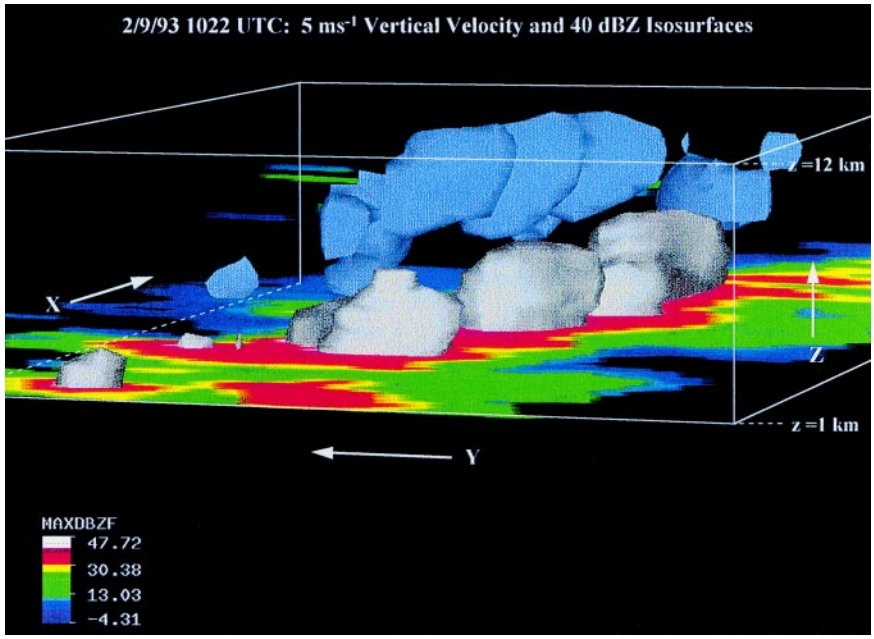


FIG. 8. Three-dimensional view of the ship case updraft and reflectivity structure at 1022 UTC. The view is from above ground and slightly behind the squall line (i.e., from the southwest). Isosurfaces of radar reflectivity ≥ 40 dBZ are indicated in white, and isosurfaces of upward vertical motion ≥ 5 m $s^{-1}$ are indicated in light blue. A Constant altitude plan position indicator (CAPPI) of radar reflectivity ($Z$ = 1 km) is plotted at the lower horizontal boundary of the figure. The maximum vertical extent of the 5 m $s^{-1}$ isosurfaces approaches 12 km. The maximum vertical extent of the 40-dBZ isosurfaces approaches 5 km.

cally. Further, as in the case of Fig. 8, updrafts greater than 5 m $s^{-1}$ (Fig. 9b) were situated just above the height of the precipitation core and above the height of the −10°C level. The observed separation of the updraft cores (≥ 5 m $s^{-1}$) from the precipitation cores (≥ 30 dBZ) between the −5° and −10°C levels suggests a significant decrease in precipitation-sized ice mass aloft and the presence of a relatively weak electrical generator (e.g., Williams et al. 1992).

To a first order, lightning production in cumulonimbus clouds is associated with a vigorous mixed-phase precipitation ice process. Indeed, perhaps the most widely accepted explanation for the generation of substantial electrical charge in thunderstorms, the "noninductive" charging (NIC) mechanism, invokes particle-scale charge separation during collisions between numerous rimed ice particles such as graupel and smaller cloud ice crystals in the presence of supercooled liquid water. Coincident cloud-scale separation of charge and the generation of breakdown electric fields is hypothesized to occur through the gravitational sedimentation of graupel, which typically carry negative charge, and the ascent of cloud ice in the updraft, which typically carries positive charge. The NIC mechanism is supported by numerous laboratory experiments, modeling studies, and observations (e.g., Workman and Reynolds 1949; Reynolds et al. 1957; Takahashi 1978; Jayaratne et al. 1983; Lhermitte and Williams 1985; Goodman et al. 1988; Dye et al. 1989; Saunders et al. 1991; Rutledge et al. 1992; Randell et al. 1994; Jameson et al. 1996).

In order for robust mixed-phase processes to develop in cumulonimbus clouds leading to efficient NIC, a "sufficiently strong" updraft must first exist in the appropriate region of the cloud. Indeed, polarimetric radar observations of highly electrified tropical cumulonimbi over Florida (e.g., Jameson et al. 1996; Ramachandran et al. 1996; French et al. 1996; Bringi et al. 1997) and the Maritime Continent region of northern Australia (Carey et al. 1997) suggest that updrafts in lightning-producing cumulonimbi provide substantial liquid water mass to the mixed-phase region of the clouds via condensation of cloud water and the lofting of millimeter-sized raindrops through the −10°C level. As the supercooled raindrops begin to freeze, rapid electrification ensues, followed by the production of lightning several minutes later (e.g., Jameson et al. 1996; Carey et al. 1997; Bringi et al. 1997). Microphysically, the frozen drops may play a dual role in the electrical charging of clouds via NIC processes by 1) providing an instantaneous graupel/small hail source upon freezing, and 2) enhancing cloud ice particle concentrations via splinter production during freezing (e.g., Takahashi and Yamashita 1997) and riming (e.g., Hallett and Mossup 1974; Mossup 1976; Chisnell and Latham 1976).

Based on balance level considerations (e.g., Atlas 1966; Lhermitte and Williams 1985) relative to the terminal fall speed of millimeter-sized liquid/frozen drops, and in situ aircraft observations of weak updraft cores in tropical oceanic convection (Zipser and LeMone 1980; Lucas et al. 1994), Zipser (1994) and Zipser and Lutz (1994) proposed that *average* updrafts of 6–7 m $s^{-1}$ occurring over a 2–3-km diameter updraft

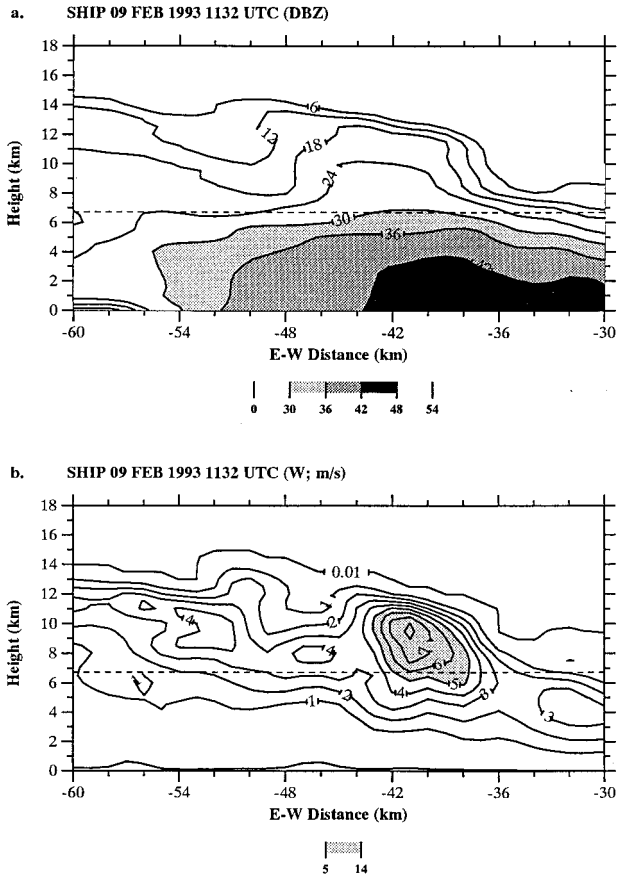


FIG. 9. Ship case cross sections (1132 UTC) of composite maximum (a) radar reflectivity and (b) upward vertical velocity taken through convection shown in Fig. 5a. The display area extends from $x = -60$ km to $x = -30$ km and represents all convection in the region between $y = 15$ and $y = 25$ km in Fig. 5a. Reflectivity values are contoured every 6 dB*Z*, and values greater than 30 dB*Z* are shaded. Velocities are contoured every 1 m s$^{-1}$ and shaded for values $\geq 5$ m s$^{-1}$. Dashed line indicates the approximate height of the −10°C isotherm.

core may be required in the 0° to −20°C region of tropical cumulonimbi to provide the appropriate concentration of precipitation-sized ice particles and mixed-phase conditions for strong electrification to occur. Note that the presence of 1–2-mm-diameter liquid and frozen drops in the 0° to −20°C temperature range in concentrations considered necessary for efficient NIC electrification to occur [e.g., $O(1\ L^{-1})$; Takahashi 1978] implies the presence of 30-dB*Z* or greater equivalent radar reflectivities near or above the −10°C temperature region. Observations reported in Petersen et al. (1996) suggest that tropical oceanic convection observed over the warm pool produced lightning only when reflectivities above the elevation of the −10°C level exceeded 30 dB*Z*, consistent with observations of lightning initiation altitudes and associated 30-dB*Z* reflectivity contours shown in Murphy et al. (1996) for Florida thunderstorms. Further, statistical analyses of 30-dB*Z* convective core heights observed over the warm pool during COARE (DeMott and Rutledge 1998a) suggest that less than 10% of tropical oceanic convective cells observed at any given time are likely to be associated with 30-dB*Z* echoes that extend above the height of the −10°C level. Interestingly, mean updraft velocities of 6–7 m s$^{-1}$ easily fall into the upper 10% of all aircraft-observed *mean* updraft magnitudes in tropical oceanic convection (Zipser and LeMone 1980; Jorsensen and LeMone 1989; Lucas et al. 1994). Hence the Zipser and Lutz (1994) "vertical velocity threshold" hypothesis has considerable (albeit indirect) observational support. The shipboard dual-Doppler observations presented herein lend further support to the above interpretation, as even *the most intense* convective cores resolved in the ship case dual-Doppler analysis (e.g., Figs. 9a,b) seldom approached the hypothesized thresholds in mixed-phase region reflectivity and/or *mean* vertical velocity required for lightning production.

## 5. Comparison of the ship case to the highly electrified aircraft case

In this section we compare dual-Doppler observations from the ship case to NOAA P-3 airborne quad-Doppler observations[3] of a lightning-producing MCS that occurred 400 km to the southeast of the ship case (4.5°S, 159°E), approximately 8 h later in the day on 9 February 1993 (e.g., Smull et al. 1994; Smull et al. 1996). Both the ship- and aircraft-observed MCSs were deep, possessing maximum echo tops of 16 and 18 km, respectively. However, the ship case produced very little lightning (one detected intracloud flash) while the aircraft case produced more than 150 cloud-to-ground (CG) lightning flashes and an uncounted number of intracloud flashes. Since multiple Doppler analyses have been completed for both MCSs, we can combine reflectivity, electricity, and diagnosed kinematic fields in a self-consistent fashion to identify important differences in storm structure between the two systems.

[3]The NCAR Electra aircraft and ELDORA radar also observed this system (e.g., Lee and Hildebrand 1995; Smull et al. 1996) but were restricted mainly to dual-Doppler observations in the far western portion of the system.

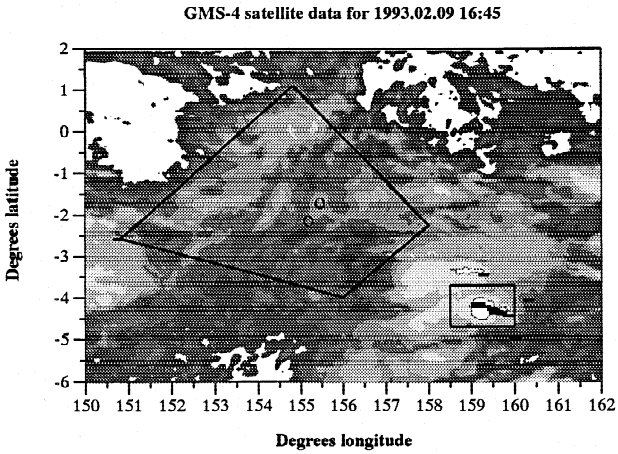


FIG. 10. *GMS-4* satellite-infrared cloud-top brightness temperatures and CG lightning locations for 9 February 1993 1645 UTC. Degrees longitude (latitude) are indicated on the abscissa (ordinate). The shading intervals, moving from dark to light, indicate temperatures less than 15°, 0°, –15°, –30°, –45°, –65°, and –80°C. The COARE IFA is indicated and the relative positions of the MIT and TOGA radars are indicated by the circles. The approximate location of the aircraft case squall line is enclosed in the box located at 159.5° and –4.5°. Bold dashes indicate the locations of CG lightning that occurred within a 30-min interval centered on 1645 UTC.

*a. Aircraft case summary*

The aircraft case (Smull et al. 1994; Lee and Hildebrand 1995; LeMone et al. 1998) was a 300-km-long intense linear MCS that formed near the southern edge of a large preexisting region of stratiform precipitation associated with an older decaying system (Fig. 10). The convective band along the leading edge of the MCS was oriented west-northwest to east-southeast, approximately perpendicular to the low-level shear vector, but parallel to the much stronger midlevel shear vector, and propagated toward the northeast at a speed of about 8 m $s^{-1}$. Due to the size of the MCS and the coordinated sampling strategy employed by the two P-3 aircraft, the structural characteristics of the system are summarized by subdividing the quad-Doppler radar analyses[4] into eastern (Fig. 11a) and western sections (Fig. 11b).

On the eastern end of the convective line (Fig. 11a), pronounced low-level storm-relative confluence of the wind occurred, with flow entering the system from both sides of the convective line. To the rear of the convective line, the flow accelerated to create a small

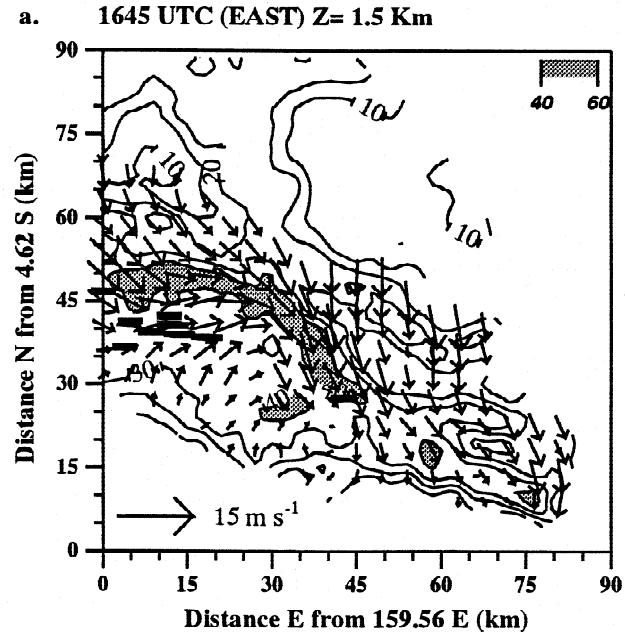


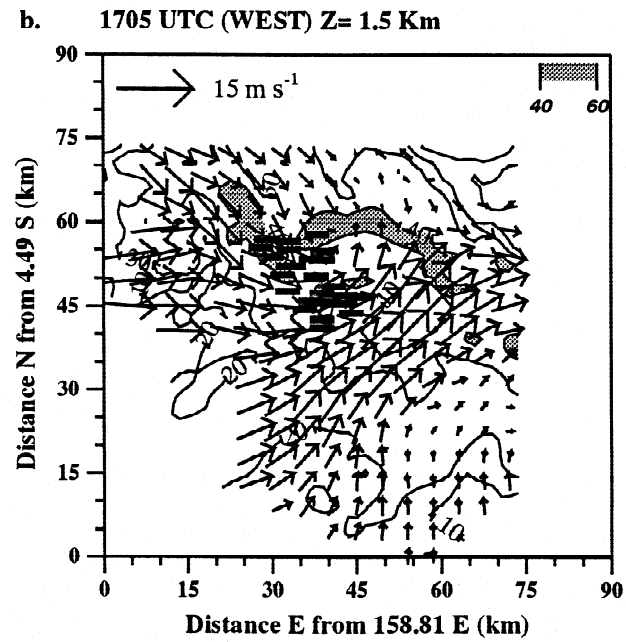


FIG. 11. Aircraft case CAPPIs of radar reflectivity (contoured every 10 dBZ) and storm-relative winds at an elevation of 1.5 km for (a) 1645 UTC, the eastern end of the squall line, and (b) 1705 UTC, the western end of the squall line. Bold dashes indicate the location of CG lightning flashes for 20-min periods centered on the time of the CAPPI. Reflectivity values ≥ 40 dBZ are shaded.

bow in the reflectivity pattern. Smull et al. (1994) determined that the inflow air in this more fully developed portion of the convective line originated primarily on the northern side of the MCS (consistent

[4]See Smull et al. (1994) and Jorgensen et al. (1996) for a summary of the analysis methodology used in airborne quad-Doppler syntheses.

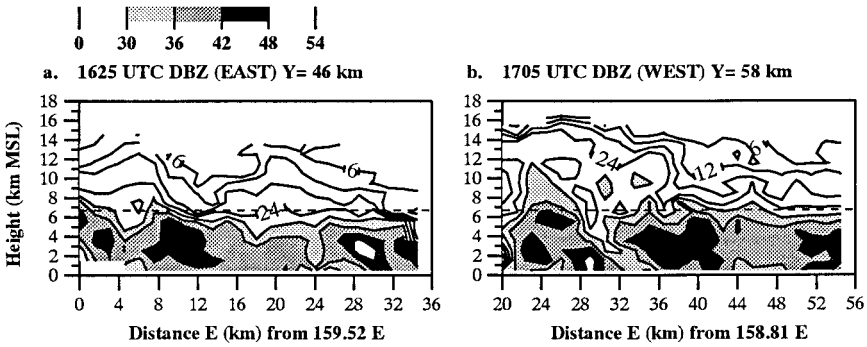


FIG. 12. As in Fig. 7a but for the aircraft case at (a) 1625 UTC $Y = 46$ km, eastern end of the squall line, and (b) 1705 UTC $Y = 58$ km, western end of the squall line.

with the direction of propagation). This is an interesting observation as the air entering the system from the north originated in a region of stratiform precipitation and, a priori, would have been expected to exhibit fairly low moist static energy. However, as detailed in section 3, the inflow environment of this MCS possessed instability similar to that of the ship case. Cloud-to-ground lightning (all negative in polarity) occurred on the eastern end of the MCS in regions where the convection was deep and vertically developed. In these areas, radar echo tops of 16–18 km were common, 30-dB*Z* reflectivities extended well into the mixed-phase region of the convective cells, and elevated reflectivity maxima (42 dB*Z*) were present in the 5–8-km layer (Fig. 12a; 1625 UTC).

Near the western edge of the quad-Doppler analysis region (Fig. 11b) both the convective and electrical intensity appeared to be stronger. A pronounced wavelike structure developed in the convective band between $x = 20$ and $x = 65$ (Fig. 11b). The sinusoidal reflectivity pattern apparently developed as the combined response to an increase in storm-relative rear inflow ($x = 45$–$60$) and associated development of a zone of lateral shear characterized by counterclockwise circulation on the western side of the rear-inflow current ($x = 37$). Cloud-to-ground lightning (all negative polarity; Fig. 11b) in this section of the storm at 1705 UTC appeared to cluster between $x = 25$ and $x = 45$ near a kink in the reflectivity pattern.[5] Reflectivities in the lightning-producing cells indicated substantial mass in the mixed-phase region of the storm (Fig. 12b), with 30-dB*Z* cores exceeding 12 km in elevation. As seen at the eastern end of the system, several cells exhibited reflectivity maxima greater than 42 dB*Z* between the −5° and −10°C levels (e.g., 6–6.5-km level in Fig. 12b), perhaps indicative of suspended hydrometeors such as supercooled raindrops and/or rimed frozen drops and graupel (e.g., Takahashi and Kuhara 1993; Bringi et al. 1997; Carey et al. 1997; Takahashi and Kawano 1998).

In an alongline cross section of maximum vertical velocity and reflectivity computed for a 15-km-wide and 30-km-long section of lightning-producing con-

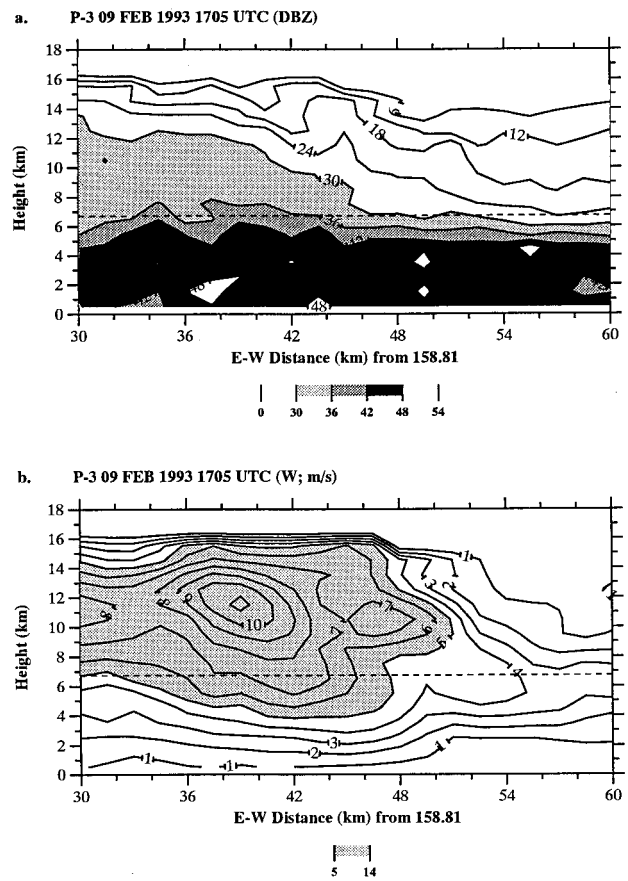


FIG. 13. As in Figs. 9a,b but for the aircraft case at 1705 UTC, western end of the squall line. (a) Maximum reflectivity composite and (b) maximum updraft composite. The cross sections include convection shown in Fig. 12b located along the segment $X = 30$ km to $X = 60$ km and between $Y = 48$ km and $Y = 61$ km.

[5]Potential errors in lightning location may approach 10 km at this range from the COARE ALDF network (e.g., Petersen et al. 1996; Koshak et al. 1998, manuscript submitted to *J. Geophys. Res.*).

vection situated on the western end of the aircraft system (Figs. 13a,b), the diagnosed updraft velocities exceeded 6 m $s^{-1}$ in reflectivity cores ≥ 30 dBZ at temperatures between 0° and –20°C (5–8 km), and were greater than 11 m $s^{-1}$ near the 12-km level. Unfortunately quad-Doppler vertical velocity measurements were not available for the deep convection located on the western edge of the analysis domain between $x$ = 20 and 28 km in Fig. 12b. However, based on the reflectivity data shown in Fig. 12b and paired vertical velocity and reflectivity data shown in Figs. 13a,b, it is reasonable to speculate that vertical velocities above the freezing level between $x$ = 20 and 28 km in Fig. 12b were similar to, or even stronger than, those shown for the cells depicted in Figs. 13a,b. Though airborne dual-Doppler radar data collected by the NCAR Electra are not shown here, it should be noted that Lee and Hildebrand (1995) reported peak updraft magnitudes of 22 m $s^{-1}$ located near the 13-km level on the far western side of the aircraft case between 1920 and 1940 UTC.

*b. Composite analyses of the ship and aircraft MCS's*

In order to more closely compare the kinematic and precipitation structures of the two systems, composite fields of vertical velocity and radar reflectivity were generated from six volumes of radar data for the ship case, and six volumes for the aircraft case over similar periods in each of the storm life cycles (1012–1212 UTC, ship case; 1614–1705 UTC, aircraft case). The composites were partitioned into "total," "convective," and "nonconvective" representations of the cloud system based on the algorithm of Steiner et al. (1995) with subsequent modifications discussed in DeMott and Rutledge (1998a) and Rickenbach and Rutledge (1998). The comparisons of vertical motion fields are complicated by the difficulty involved in selecting radar volumes from each cloud system that represent similar stages of convective evolution, and also by potential errors introduced through the use of different measurement platforms, sampling strategies, filtering, and wind-synthesis techniques [e.g., dual- vs quad-Doppler syntheses; Jorgensen et al. (1996)]. For example, dual-Doppler syntheses were completed for all of the shipborne data, while four of the six volumes of P-3 data composited represent quad-Doppler analyses. Analyses of the vertical motion composites do indeed exhibit a certain degree of consistency when considered with concomitant reflectivity and lightning observations; however, *a note of caution is certainly warranted regarding their interpretation from a quantitative standpoint.*

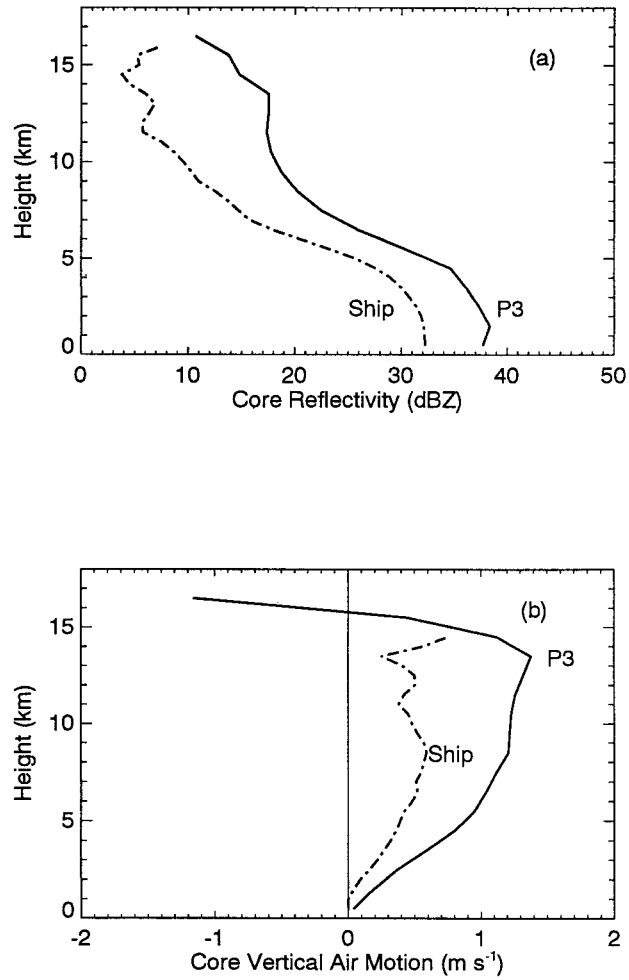


FIG. 14. Composited vertical profiles of *convective region* (a) radar reflectivity and (b) upward motion for the ship (dash–dot line) and aircraft cases (solid line). Radar reflectivity in (a) and upward motion in (b) are plotted on the abscissa, height on the ordinate.

Composite vertical profiles of radar reflectivity and vertical velocity in the *convective* regions[6] for the ship and aircraft cases are compared in Figs. 14a,b. The marked differences in mean convective reflectivity profile between the two systems (Fig. 14a) are consistent with that noted to exist between the kinematic and electrical properties of the two systems, and are also similar to differences noted by Rutledge et al. (1992),

[6]Discussion of the stratiform and total vertical motion composites are deferred to a forthcoming paper that examines storm kinematics in much greater detail.

Williams et al. (1992), and Zipser and Lutz (1994) for tropical continental (highly electrified) and monsoon (weakly electrified) vertical profiles of radar reflectivity. Note that the absolute difference in reflectivity between the two systems at each elevation diverges with height, the aircraft case possessing reflectivities ~6 dB$Z$ greater than the ship case at 5 km and ~10 dB$Z$ greater at a height of 10 km. The increasing difference in reflectivity with height above 5 km in Fig. 14a suggests that a significant fraction of the convection sampled in the aircraft case was associated with larger ice particles in the mixed-phase region of the cloud.

With regard to the vertical velocity profiles, Fig. 14b suggests that larger vertical velocities occurred over the entire depth of the convection sampled by aircraft relative to the ship case, consistent with the observed differences in reflectivity structure and electrical intensity. In comparison to the ship case profile of vertical velocity, the convective updraft profile of the aircraft case exhibited a more rapid increase with respect to height, 50% greater vertical velocities above 5 km, and a single peak in the updraft occurring near a height of 12 km. The stronger updraft in the aircraft case suggests that convective cores in the aircraft-observed MCS may have been better able to support the growth of large, fast-falling hydrometeors (e.g., liquid/frozen drops) as they ascended above the freezing level.

*c. Discussion*

Both the ship and aircraft case soundings exhibited similar CAPE and shear (Figs. 2a,b). Yet the multiple Doppler analyses suggest that the aircraft case exhibited a larger degree of low-level forcing, maximum echo tops of 18 km, stronger updrafts and higher reflectivities in the mixed-phase region of the cloud, and a relatively high degree of electrification as evidenced by lightning observations. Conversely, convection in the ship case, while associated with maximum echo-top heights on the order of 16 km, was associated with relatively weak forcing, weak vertical development above the –5°C level, moderate electric fields at the surface, and very little detectable lightning. These differences in kinematic and precipitation structure were further manifested in composited vertical profiles of the mean convective precipitation and vertical velocity structure (Figs. 14a,b).

"Snapshots" of the diagnosed updraft magnitudes in the 0° to –10°C region of both systems differed by several meters per second in the mean (e.g., Figs. 7b, 9b, and 13b), and these differences were apparently significant from both a microphysical and electrical viewpoint. In the highly electrified cells of the aircraft case, peak diagnosed updrafts below the base of the mixed-phase region (–5° to –10°C) appeared to be greater than or equal to 6 m $s^{-1}$. Conversely, maximum vertical velocities diagnosed for the ship case were almost always less than 6 m $s^{-1}$ in the lower portion of the mixed-phase region. To the extent that the dual- and quad-Doppler vertical velocities are representative of the mean convective updraft structure in each case, millimeter-sized supercooled and frozen raindrops with terminal fall speeds on the order of 5–7 m $s^{-1}$ (Zipser and Lutz 1994) could have been lofted into the mixed-phase region of the aircraft case and maintained at higher elevations as the particles grew by riming, given general increases in vertical velocity with height (e.g., Fig. 14b). Furthermore, the stronger updrafts (e.g., Figs. 13b, 14b) characteristic of the aircraft case should have generated more supercooled cloud water, creating mixed-phase conditions conducive to the riming growth of graupel and frozen drops and, hence, more efficient precipitation-based charge generation in the storm (e.g., Takahashi 1978; Saunders et al. 1991).

## 6. Conclusions

This study has presented an overview of ship-based dual-Doppler observations conducted during TOGA COARE, set in the framework of a case study analysis. Observations of the kinematic and precipitation structure of a squall line sampled by the MIT and TOGA radars on 9 February 1993 were compared to another similarly organized but more intense MCS, observed by NOAA P-3 airborne Doppler radars on the same day. The case study analyses presented herein focused on the relationship between storm kinematics, precipitation structure, microphysics, and electrification as observed in tropical oceanic convection occurring over remote regions of the western Pacific warm pool. Companion papers to be submitted in the future will expand on this study by discussing in much greater detail the spatial and temporal characteristics of momentum transports as related to convective line orientation and wind shear (e.g., Lafore et al. 1988; LeMone and Moncrieff 1994), diabatic heating budgets, and numerically simulated dynamical, microphysical, and electrical properties of the convection.

To some extent the shipboard dual-Doppler operations during TOGA COARE were conducted as an

experiment to examine the feasibility of conducting dual-Doppler operations at sea (e.g., given radar stabilization requirements, sampling geometry, location, etc.). Given the success of shipborne dual-Doppler operations during sampling of the 9 February 1993 squall line, the study of storm reflectivity and kinematic structures appears to be completely feasible using conventional dual-Doppler techniques with shipborne radars. If provided the opportunity, future field programs over the tropical oceans should include dedicated shipboard dual-Doppler scanning.

*Acknowledgments.* We would like to thank other members of the *PRC5* and R/V *Vickers* radar scientist staff who were crucial to the successful completion of shipborne dual-Doppler operations during February of 1993: *PRC5*—P. Istvan, D. Wolff, and R. Barritt; R/V *Vickers*—Dr. D. Boccippio, Dr. A. Doggett, J. Lutz, and I. Savage. The NOAA Officer Corp and University of Southern California members of the R/V *Vickers* crew are also acknowledged for their professionalism and cooperation during TOGA COARE. Dr. Jeff Halverson is acknowledged for preparation of the sounding hodographs and stimulating discussion. Dr. M. LeMone, Prof. E. Zipser, and an anonymous reviewer are acknowledged for their helpful comments during preparation of this manuscript. This research was supported under grants to CSU provided by NOAA Grant NA67RJ0152 and NASA Grant NAG5-4754.

## References

Alexander, G. D., and G. S. Young, 1992: The relationship between EMEX mesoscale precipitation feature properties and their environmental characteristics. *Mon. Wea. Rev.,* **120,** 554–564.

Ascencio, N., J. P. Lafore, P. Pires, and J. L. Redelsperger, 1993: Analyses quitidiennes du cepmmt durant la periode d'observations intensives de l'experience TOGA/COARE. Note de travail, Groupe de meteorologie a moyenne echelle 12, Centre National de Recherches Meteorologiques, Tolouse, France, 243 pp.

Atlas, D. A., 1966: The balance level in convective storms. *J. Atmos. Sci.,* **23,** 635–651.

Bond, G., and D. Alexander, 1994: *TOGA COARE Meteorological Atlas.* Tech. Rep., UCAR/TOGA COARE International Project Office. [Available from UCAR/TCIPO, UCAR Communications, P. O. Box 3000, Boulder, CO 80307.]

Bringi, V. N., K. Knupp, A. Detwiler, L. Liu, I. J. Caylor, and R. A. Black, 1997: Evolution of a Florida thunderstorm during the Convection and Precipitation/Electrification Experiment: The case of 9 August 1991. *Mon. Wea. Rev.,* **125,** 2131–2160.

Carey, L. D., S. A. Rutledge, W. A. Petersen, and T. D. Keenan, 1997: C-Band polarimetric radar and electrical observations of a maritime continent thunderstorm. Preprints, *22d Conf. on Hurricanes and Tropical Meteorology,* Fort Collins, CO, Amer. Meteor. Soc., 384–385.

Chisnell, R. F., and Latham, 1976: Ice particle multiplication in cumulus clouds. *Quart. J. Roy. Meteor. Soc.,* **102,** 133–156.

DeMott, C. A., and S. A. Rutledge, 1988a: The vertical structure of TOGA COARE convection: Radar echo distributions. *J. Atmos. Sci.,* **55,** 2730–2747.

——, and ——, 1998b: The vertical structure of TOGA COARE convection. Part II: Moduating influences and implications for diabatic heating. *J. Atmos. Sci.,* **55,** 2748–2762.

Dye, J. E., J. J. Jones, A. J. Weinheimer, and W. P. Winn, 1989: Observations within two regions of charge during initial thunderstorm electrification. *Quart. J. Roy. Meteor. Soc.,* **114,** 1271–1290.

Ferrier, B. S., J. Gerlach, P. Kucera, D. Short, S. Rutledge, J. Lutz, and O. Thiele, 1995: Corrections and comparisons of TOGA COARE shipborne radar reflectivities. Preprints, *27th Conf. on Radar Meteorology,* Vail, CO, Amer. Meteor. Soc., 675–677.

French, J. R., J. H. Helsdon, A. G. Detwiler, and P. L. Smith, 1996: Microphysical and electrical evolution of a Florida thunderstorm. 1. Observations. *J. Geophys. Res.,* **101,** 18 961–18 977.

Goodman, S. J., D. E., Buechler, P. D. Wright, and W. D. Rust, 1988: Lightning and precipitation history of a microburst-producing storm. *Geophys. Res. Lett.,* **15,** 1185–1188.

Hallett, J., and S. C. Mossop, 1974: Production of secondary ice crystals during the riming process. *Nature,* **249,** 26–28.

Hildebrand, P. H., and Coauthors, 1996: The ELDORA/ASTRIA airborne Doppler weather radar: High-resolution observations from TOGA COARE. *Bull. Amer. Meteor. Soc.,* **77,** 213–232.

Houze, R. A., Jr., and C.-P. Cheng, 1977: Radar characteristics of tropical convection during GATE: Mean properties and trends over the summer season. *Mon. Wea. Rev.,* **105,** 964–980.

Jameson, A. R., M. J. Murphy, and E. P. Krider, 1996: Multiparameter radar observations of isolated Florida cumulonimbi during the onset of electrification. *J. Appl. Meteor.,* **35,** 343–354.

Jayaratne, E. R., C. P. R. Saunders, and J. Hallett, 1983: Laboratory studies of the charging of soft hail during ice crystal interactions. *Quart. J. Roy. Meteor. Soc.,* **109,** 609–630.

Jorgensen, D. P., and M. A. LeMone, 1989: Vertical velocity characteristics of oceanic convection. *J. Atmos. Sci.,* **46,** 621–640.

——, ——, and B. J.-D. Jou, 1991: Precipitation and kinematic structure of an oceanic mesoscale convective system. Part I: Convective line structure. *Mon. Wea. Rev.,* **119,** 2608–2637.

——, T. Matejka, and J. D. DuGranrut, 1996: Multi-beam techniques for deriving wind fields from airborne Doppler radars. *J. Meteor. Atmos. Phys.,* **59,** 83–104.

——, M. A. LeMone, and S. B. Trier, 1997: Structure and organization of the 22 February 1993 TOGA COARE squall line: Aircraft observations of precipitation, circulation, and surface energy fluxes. *J. Atmos. Sci.,* **54,** 1961–1985.

Lafore, J.-P., J.-L. Redelsperger, and G. Jaubert, 1988: Comparison between a three-dimensional simulation and Doppler radar data of a tropical squall line: Transports of mass, momentum, heat and moisture. *J. Atmos. Sci.,* **45,** 3483–3500.

Leary, C. A., and R. A. Houze Jr., 1979: The structure and evolution of convection in a tropical cloud cluster. *J. Atmos. Sci.,* **36,** 437–457.

——, A. L. Doggett IV, and G. M. Jurica, 1993: Navigational uncertainties in the TOGA COARE shipboard radar data: Implications for echo locations and Doppler velocities. Rep. to

TOGA COARE International Project Office, 20 pp. and appendix (263 pp). [Available from UCAR Communications, P. O. Box 3000, Boulder, CO 80307-3000.]

Lee, W.-C., and P. H. Hildebrand, 1995: Kinematic and thermodynamic structure of a TOGA COARE squall line retrieved from the ELDORA data. Preprints, *27th Conf. on Radar Meteorology,* Vail, CO, Amer. Meteor. Soc., 811–813.

LeMone, M. A., and M. W. Moncrieff, 1994: Momentum and mass transport by convective bands: Comparisons of highly idealized dynamical models to observations. *J. Atmos. Sci.,* **51,** 281–305.

——, E. J. Zipser, and S. B. Trier, 1998: The role of environmental shear and thermodynamic conditions in determining the structure and evolution of mesoscale convective systems during TOGA COARE. *J. Atmos. Sci.,* in press.

Lhermitte, R., and E. Williams, 1985: Thunderstorm electrification: A case study. *J. Geophys. Res.,* **90,** 6071–6078.

Lucas, C., E. J. Zipser, and M. A. LeMone, 1994: Vertical velocity in oceanic convection off tropical Australia. *J. Atmos. Sci.,* **51,** 3184–3193.

Marks, F. D., Jr., and R. A. Houze Jr., 1984: Airborne Doppler radar observations in Hurricane Debby. *Bull. Amer. Meteor. Soc.,* **65,** 569–582.

Matejka, T., and S. A. Lewis, 1997: Improving research aircraft navigation by incorporating INS and GPS information in a variational solution. *J. Oceanic Atmos. Technol.,* **14,** 495–511.

Mohr, C. G., and L. J. Miller, 1983: CEDRIC—A software package for Cartesian space editing, synthesis, and display of radar fields under interactive control. Preprints, *21st Conf. on Radar Meteorology,* Edmonton, AB, Canada, Amer. Meteor. Soc., 559–574.

Mossup, C. S., 1976: Production of secondary ice particles during growth of graupel by riming. *Quart. J. Roy. Meteor. Soc.,* **102,** 54–57.

Murphy, M. J., E. P. Krider, and M. W. Maier, 1996: Lightning charge analyses in small Convection and Precipitation Electrification (CaPE) experiment storms. *J. Geophys. Res.,* **101,** 29 615–29 626.

O'Brien, J. J., 1970: Alternative solutions to the classical vertical velocity problem. *J. Appl. Meteor.,* **9,** 197–203.

Orville, R. E., and D. W. Spencer 1979: Global lightning flash frequency. *Mon. Wea. Rev.,* **107,** 934–943.

——, and Coauthors, 1997: Lightning in the region of the TOGA COARE. *Bull. Amer. Meteor. Soc.,* **78,** 1055–1067.

Petersen, W. A., S. A. Rutledge, and R. E. Orville, 1996: Cloud-to-ground lightning observations in TOGA COARE: Lightning location algorithms and selected results. *Mon. Wea. Rev.,* **124,** 602–620.

Ramachandran, R., A. Detwiler, J. Helsdon Jr., P. L. Smith, and V. N. Bringi, 1996: Precipitation development and electrification of Florida thunderstorm cells during Convection and Precipitation/Electrification Project. *J. Geophys. Res.,* **101,** 1599–1619.

Randell, S. C., S. A. Rutledge, R. D. Farley, and J. H. Helsdon, 1994: A modeling study of the early electrical development of tropical convection: Continental and oceanic (monsoon) storms. *Mon. Wea. Rev.,* **122,** 1852–1877.

Ray, P. S., C. L. Ziegler, and W. Baumgarner, 1980: Single and multiple Doppler radar observations of tornadic storms. *Mon. Wea. Rev.,* **108,** 1607–1625.

Reynolds, S. E., M. Brook, and M. F. Gourley, 1957: Thunderstorm charge separation. *J. Meteor.,* **14,** 426–436.

Rickenbach, T. M., and S. A. Rutledge, 1998: Convection in TOGA COARE: Horizontal scale, morphology, and rainfall production. *J. Atmos. Sci.,* **55,** 2715–2729.

Rutledge, S. A., E. R. Williams, and T. D. Keenan, 1992: The Down Under Doppler and Electricity Experiment (DUNDEE): Overview and preliminary results. *Bull. Amer. Meteor. Soc.,* **73,** 3–16.

——, and Coauthors, 1993: The shipboard deployment of the MIT C-band radar during TOGA COARE. Preprints, *26th Int. Conf. on Radar Meteorology,* Norman, OK, Amer. Meteor Soc., 371–373.

Saunders, C. P. R., W. D. Keith, and R. P. Mitzeva, 1991: The effect of liquid water on thunderstorm charging. *J. Geophys. Res.,* **96,** 11 007–11 017.

Short, D. A., P. A. Kucera, B. S. Ferrier, J. C. Gerlach, S. A. Rutledge, and O. W. Thiele, 1997: Shipboard radar rainfall patterns within the TOGA COARE IFA. *Bull. Amer. Meteor. Soc.,* **78,** 2817–2836.

Smull, B. F., D. P. Jorgensen, T. J. Matejka, and M. A. LeMone, 1994: Evolution of precipitation and momentum structure within a slow moving convective band observed by airborne Doppler radar during TOGA COARE. Preprints, *Sixth Conf. on Mesoscale Processes,* Portland, OR, Amer. Meteor. Soc., 21–24.

——, T. J. Matejka, and M. A. LeMone, 1996: Airflow trajectories within a slow-moving convective system observed during TOGA COARE. Preprints, *Seventh Conf. on Mesoscale Processes,* Reading, United Kingdom, Amer. Meteor. Soc., 289–291.

Steiner, M., R. A. Houze Jr., and S. E. Yuter, 1995: Climatological characterization of three-dimensional storm structure from operational radar and rain gauge data. *J. Appl. Meteor.,* **34,** 1978–2007.

Szoke, E. J., and E. J. Zipser, 1986: A radar study of convective cells in mesoscale systems in GATE. Part II: Life cycles of convective cells. *J. Atmos. Sci.,* **43,** 199–218.

——, ——, and D. P. Jorgensen, 1986: A radar study of convective cells in mesoscale systems in GATE. Part I: Vertical profile statistics and comparison with hurricanes. *J. Atmos. Sci.,* **43,** 182–197.

Takahashi, C., and A. Yamashita, 1977: Production of ice splinters by the freezing of water drops in free fall. *J. Meteor. Soc. Japan,* **55,** 139–141.

Takahashi, T., 1978: Riming electrification as a charge generation mechanism in thunderstorms. *J. Atmos. Sci.,* **35,** 1536–1548.

——, and K. Kuhara, 1993: Precipitation mechanisms of cumulonimbus clouds at Pohnpei, Micronesia. *J. Meteor. Soc. Japan,* **71,** 21–31.

——, and T. Kawano, 1998: Numerical sensitivity study of rainband precipitation and evolution. *J. Atmos. Sci.,* **55,** 57–87.

Webster, P. J., and R. Lukas, 1992: TOGA COARE: The Coupled Ocean–Atmosphere Response Experiment. *Bull. Amer. Meteor. Soc.,* **73,** 1377–1416.

Williams, E. R., S. A. Rutledge, S. C. Geotis, N. Renno, E. Rasmussen, and T. Rickenbach, 1992: A radar and electrical study of tropical hot towers. *J. Atmos. Sci.,* **49,** 1386–1395.

Workman, E. J., and S. E. Reynolds, 1949: Electrical activity as related to thunderstorm cell growth. *Bull. Amer. Meteor. Soc.,* **30,** 142–149.

Yuter, S. E., R. A. Houze Jr., B. F. Smull, F. D. Marks Jr., J. R. Daugherty, and S. R. Brodzik, 1995: TOGA COARE aircraft mission summary images: An electronic atlas. *Bull. Amer. Meteor. Soc.*, **76,** 319–328.

Zipser, E. J., 1994: Deep cumulonimbus cloud systems in the Tropics with and without lightning. *Mon. Wea. Rev.*, **122,** 1837–1851.

——, and M. A. LeMone, 1980: Cumulonimbus vertical velocity events in GATE. Part II: Synthesis and model core structure. *J. Atmos. Sci.*, **37,** 2458–2469.

——, and K. R. Lutz, 1994: The vertical profile of radar reflectivity of convective cells: A strong indicator of storm intensity and lightning probability? *Mon. Wea. Rev.*, **122,** 1751–1759.

# corrigenda

In the article "High-Resolution Wind Fields within the Inner Core and Eye of a Mature Tropical Cyclone from GOES 1-min Images" by A. F. Hasler et al., which appeared in the November 1998 issue of the *Bulletin,* the author affiliations were incorrect. The correct affiliations are as follows:

A. F. Hasler, NASA/Goddard Space Flight Center, Greenbelt, Maryland.
K. Palaniappan, Department of Computer Engineering and Computer Science, University of Missouri, Columbia, Missouri.
C. Kambhammetu, Department of Computer and Information Science, University of DElaware, Newark, Delaware.
P. Black, Hurricane Research Division, Atlantic Oceanographic and Meteorological Laboratories, NOAA, Miami, Florida.
E. Uhlhorn, Hurricane Research Division, Atlantic Oceanographic and Meteorological Laboratories, NOAA, Miami, Florida.
D. Chesters, NASA/Goddard Space Flight Center, Greenbelt, Maryland.

The *Bulletin* apologizes for this error.

In the October 1998 *Bulletin,* the credit for the photo on page 2184 was inadvertently omitted. The photo was provided courtesy of Lotta Hjorth.